ACS APPLIED MATERIALS & INTERFACES

Research Article

www.acsami.org

2D Hybrid Nanostructure of Reduced Graphene Oxide–CdS Nanosheet for Enhanced Photocatalysis

Rajesh Bera, Simanta Kundu, and Amitava Patra*

Department of Materials Science, Indian Association for the Cultivation of Science, Kolkata 700 032, India

Supporting Information

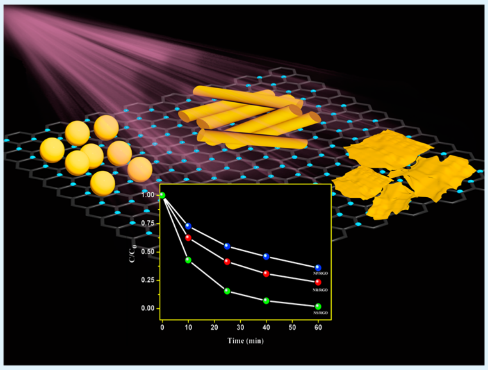

ABSTRACT: Graphene-based hybrid nanostructures have recently emerged as a new class of functional materials for light-energy conversion and storage. Here, we have synthesized reduced graphene oxide (RGO)−semiconductor composites to improve the efficiency of photocatalysis. Zero-dimensional CdS nanoparticles (0D), one-dimensional CdS nanorods (1D), and two-dimensional CdS nanosheets (2D) are grafted on the RGO sheet (2D) by a surface modification method using 4-aminothiophenol (4-ATP). Structural analysis confirms the attachment of CdS nanocrystals with RGO, and the strong electronic interaction is found in the case of a CdS nanosheet and RGO, which has an influence on photocatalytic properties. The degradation of dye under visible light varies with changing the dimension of nanocrystals, and the catalytic activity of the CdS NS/RGO composite is ~4 times higher than that of CdS nanoparticle/RGO and 3.4 times higher than that of CdS nanorod/RGO composite samples. The catalytic activity of the CdS nanosheet/RGO composite is also found to be ~2.5 times than that of pure CdS nanosheet samples. The unique 2D−2D nanoarchitecture would be effective to harvest photons from solar light and transport electrons to reaction sites with respect to other 0D−2D and 1D−2D hybrid systems. This observation can be extended to other graphene-based inorganic semiconductor composites, which can provide a valuable opportunity to explore novel hybrid materials with superior visible-light-induced catalytic activity.

KEYWORDS: *graphene, CdS nanoparticle, CdS nanorod, CdS nanosheet, nanocomposite, photocatalysis*

INTRODUCTION

In recent years, solar energy is being used for light-induced chemical transformation or generation of electricity such as photocatalysis, photovoltaics, catalytic hydrogen generation, and energy storage applications. Carbon-based materials such as carbon nanotubes (CNTs), fullerenes, graphene, carbon dots, and also graphite-like hexagonal boron nitride (BN) have opened up new frontiers in materials for development of clean and renewable energy conversion and energy storage systems.[1−5] In particular, graphene is a potential material to accumulate, store, and transport photogenerated electrons and excitons from the semiconductor or other fluorescence molecules to promote the efficiency of photoinduced activity because of its unique 2D single atomic layer, superior conductivity, charge mobility, and optoelectronic properties.[6−11]

On the other hand, one-dimensional (1D) and two-dimensional (2D) (nanorods, nanowires, nanotubes, and nanosheet) semiconducting nanostructures are thought to play a crucial role in next-generation building blocks for solar energy harvesting and photocatalysis, due to their fascinating physicochemical properties and their unique geometric and electronic properties.[12−20] Emphasis has been given on wide-band-gap semiconductor nanomaterials, such as TiO_2- and ZnO-based nanostructures,[21,22] which exhibit ultraviolet region absorption instead of visible light harvesting. However, a II−IV semiconductor, such as CdS, has a suitable band gap (2.4 eV), which is appropriate for sunlight absorption.[23,24] Thus, CdS-based hybrid systems are used for the sunlight harvesting, where CdS acts as a light harvester.[25,26] Fang and his co-workers developed a CdS nanosphere−Au hybrid system for efficient photocatalytic degradation of dye.[27] Xu and his co-workers used a CdS@TiO_2[28] nanostructure, which was found to be a good catalyst for organic transformation. Interestingly, a CdS nanosheet is being used for visible-light-driven water splitting.[16]

Now-a-days, significant attention has been given to develop semiconductor-based heterostructures and composite systems for visible-light-driven light harvesting systems. Special emphasis has been given on designing reduced graphene oxide (RGO)−semiconductor composites[29−39] to improve the efficiency of the catalyst, because the semiconductor materials can be attached with the reduced graphene oxide surface and photogenerated electrons can be extracted easily to graphene. Lee et al. reported a highly photoactive and low-band-gap TiO_2−graphene composite.[40] The photocatalytic activity of graphene−TiO_2 nanowire and nanoparticle composites is investigated.[41] A CdS quantum dot−graphene composite is

Received: January 6, 2015
Accepted: June 1, 2015
Published: June 1, 2015

DOI: 10.1021/acsami.5b03800
ACS Appl. Mater. Interfaces 2015, 7, 13251−13259

being used for photoelectrochemical and photocatalytic applications.[42] H_2 gas generation under visible light irradiation has been demonstrated by using a CdS cluster−graphene sheet composite.[43] Xu and his co-workers[44] fabricated graphene sheet and CdS nanowire composites for selective reduction of nitro compounds under visible light irradiation. The influence of size on electron transfer from CdTe quantum dots to graphene oxide in a CdTe/graphene oxide system has been investigated by using time-resolved spectroscopy,[45] and it is found that a size-dependent electron transfer process plays a crucial role in the visible-light-driven reduction process. Thus, several studies have been performed by varying the size and morphology of the semiconducting component for tuning the catalytic property in the hybrid systems. Thus, it is expected that the photocatalytic property of the GO−semiconductor composites can be tuned by changing the morphology of nanomaterials (0D, 1D, or 2D).

Herein, we have designed three different RGO composite systems where a two-dimensional (2D) CdS nanosheet (NS), one-dimensional (1D) nanorod (NR), and zero-dimensional (0D) nanoparticle (NP) are attached individually on a 2D RGO nanosheet by a surface modification method using 4-aminothiophenol (4-ATP). These composites are characterized by powder X-ray diffraction (XRD), transmission electron spectroscopy (TEM), Fourier transform infrared spectroscopy (FT-IR), Raman spectroscopy, UV−vis diffused reflectance spectroscopy (DRS), and photoluminescence. Finally, we investigate the influence of CdS morphology on the photocatalytic properties under visible-light-induced degradation of Methylene Blue (MB) dye molecules. Analysis reveals that CdS nanosheet (2D)−RGO (2D) composite exhibits efficient photocatalytic properties than other dimensions. This provides a new 2D−2D architecture of CdS/RGO composites for efficient photodriven applications.

■ EXPERIMENTAL SECTION

Materials. Sodium diethyldithiocarbamate ($C_5H_{10}NS_2Na$), cadmium chloride, and 4-aminothiophenol (4-ATP) were purchased from Sigma-Aldrich. Diethylenetriamine (DETA), graphite powder (60 mesh), sulfuric acid (H_2SO_4), nitric acid (HNO_3), hydrochloric acid (HCL), potassium persulfate ($K_2S_2O_8$), phosphorus pentoxide (P_2O_5), hydrogen peroxide (H_2O_2), potassium permanganate ($KMnO_4$), and ethanol were obtained from Merck India Ltd. All chemicals are of analytical grade and used without further purification.

Synthesis of Graphene Oxide. Graphene oxide (GO) was obtained using the modified Hummer's method.[46] Briefly, 3 g of graphite powder was mixed with 1.5 g of $NaNO_3$ (Merck) and 50 mL of cold H_2SO_4, and the mixture was cooled down to 0 °C. Then, 9 g of $KMnO_4$ was added slowly, maintaining the temperature below 5 °C. The cooling bath was removed; then, the mixture was stirred at room temperature for half an hour. Then, 100 mL of water was added and the temperature was increased to 90 °C and kept there for 1 h. The mixture was diluted with another 300 mL of water, and then 20 mL of 30% H_2O_2 solution was treated until the effervescence was ceased. The solution was left for overnight, and then the supernatant was decanted. The brown precipitate was centrifuged and washed with 10% HCl solution for several times and finally with water. The product was dispersed in water by sonication for 45 min, and then large particles were centrifuged out at 3000 rpm. The remaining particles were centrifuged at 12 000 rpm and collected and dried at vacuum. Next, 5 mg of this powder was dispersed in 10 mL of deionized water by sonication, giving rise to a 0.5 mg/mL brown dispersion of GO which was stable for months.

Synthesis of CdS NPs. CdS nanoparticles were synthesized[47] by a previously reported method. In brief, 0.266 g of cadmium acetate was added in a 25 mL round-bottom flask containing 8 mL of oleylamine with degassing for 20 min at 150 °C. In another round-bottom flask, 0.032 g sulfur powder was added into 4 mL of oleylamine with stirring until it dissolved completely. Then, the S precursor was gently added to the Cd precursor at 150 °C and stirred for 2 h. Reaction was stopped by adding toluene and washing with an ethanol−hexane mixture for three times. After drying at 60 °C in a vacuum oven, 50 mg of NP and 25 mg of 4-ATP were added in 50 mL of a 1:1 water−ethanol mixture, maintaining pH 6 in a 100 mL round-bottom flask. The mixture was stirred overnight at room temperature in an inert atmosphere. The product was centrifuged and washed with ethanol to remove excess ligands. Thus, surface modification of CdS NPs was achieved.

Synthesis of CdS NRs. CdS nanorods were synthesized by a modified method which is previously reported.[44] Briefly, 0.073 g of cadmium diethyl dithiocarbamate was added to a 20 mL Teflon-lined stainless steel autoclave. Then, 13 mL of DETA was added, and the mixture was maintained 180 °C for 24 h. After that, the autoclave was cooled to room temperature. The yellowish product was centrifuged and washed for several times with a water−ethanol mixture and dried at 60 °C in a vacuum oven. The surface of the CdS NRs was modified by 4-ATP by the following procedure: 50 mg of NR and 25 mg 4-ATP were added in a 100 mL RB containing 50 mL of a 1:1 water−ethanol mixture under an argon atmosphere at pH 6. After stirring overnight, it was centrifuged with ethanol and dried in a vacuum.

Synthesis of CdS NSs. CdS nanosheets were synthesized following a reported method.[16] In brief, 0.32 mmol of $CdCl_2 \cdot 2.5H_2O$, 2 mmol of sulfur powder, and 12 mL of DETA were stirred in a 50 mL round-bottom flask for 10 min. Then, it was loaded and sealed in a Teflon-lined autoclave having a capacity of 20 mL. The autoclave was heated at 80 °C for 48 h. After that, it was cooled to room temperature, and a light yellow product was collected by centrifugation. It was washed several times with ethanol and distilled water and dried at 60 °C in a vacuum oven. The surface modification of these nanosheets was achieved by the following method: 50 mg of these dried NSs and 25 mg of 4-ATP were added in 50 mL of an ethanol−water (1:1) solution mixture at pH 6. Then, it was sonicated for 1 h under a low-power sonic bath in an inert atmosphere and left undisturbed for 3 h. The unexfoliated NSs were settled down and the upper portion of the container was collected. This was centrifuged and washed for several times and dried in a vacuum oven.

Synthesis of CdS NP/NR/NS−RGO Composites. Composites of CdS nanostructures with RGO are prepared via a two-step method. First, the surface-functionalized nanostructures were added with negatively charged GO to form a composite. Then, a typical hydrothermal method was used for reduction of GO to RGO using hydrazine hydrate. In brief, 50 mg of as-prepared functionalized NSs was dissolved in 12 mL of a 3:1 water−ethanol mixture. Then, 2 mg of GO was added to the above solution under mild sonication. This suspension was stirred for 30 min. After centrifugation, the suspension was redispersed in 12 mL of deionized water. The pH of the solution was adjusted to 9, and 100 μL of hydrazine hydrate was added. The mixture was transferred to a Teflon-lined autoclave of 20 mL capacity, and the autoclave was placed in a oven at 80 °C for 2 h. The yellow-greenish product was collected by centrifugation and washed with deionized water for 3 times. The obtained NS/RGO composite was dried at 60 °C in a vacuum oven. A schematic representation of the composite preparation is shown in Scheme 1. The same procedure was followed for the preparation of NP/RGO and NR/RGO composites and stored for further characterization. For comparison with composite systems, pure CdS nanocrystals were prepared by using a similar hydrothermal condition.

Characterization. X-ray diffraction (XRD) study was performed using a Cu Kα source (1.5418 Å) radiation (Siemens model D500) to identify the crystallinity of CdS NP, CdS NR, CdS NS, and their composites with RGO. The morphological study of as-synthesized hybrid nanostructures was characterized by transmission electron microscopy using a JEOL, JEM-2100F at an operating voltage of 200 kV, and AFM study was done by using a VEECO, dicp-II instrument. Raman spectra were performed on a Horiba Jobin Yvon, T64000 model, exciting the samples by a 514 nm laser beam. Fourier-transform infrared (FTIR) spectroscopy measurements were performed on a

Scheme 1. Schematic Representation of the Preparation of CdS NS/RGO Composite

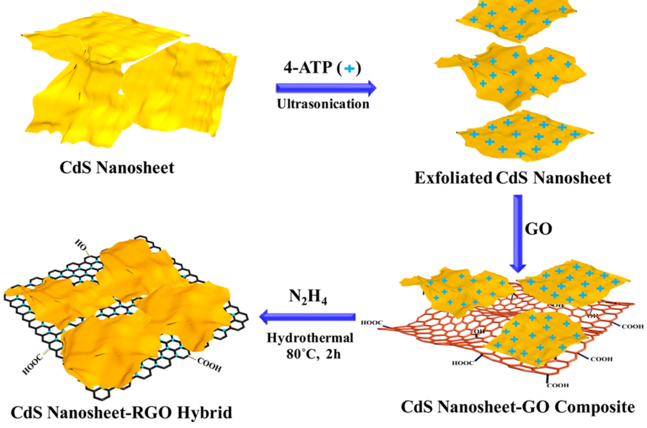

SHIMADZU made FTIR-8300 spectrometer using KBr pellets. The XPS measurements were carried out by using an Omicron Nanotechnology instrument. Zeta potential was measured with a Malveron Zetasizer instrument. Room-temperature optical absorption spectra were taken by a UV−vis spectrophotometer (Shimadzu). Room-temperature photoluminescence studies were carried out using a Fluoro Max-P (Horiba Jobin Yvon) luminescence spectrophotometer. LC−MS (liquid chromatography−mass spectrometry) study was done by using a Waters 3100 mass detector.

Photocatalytic activity of as-prepared CdS (NP, NR, and NS) and their RGO composite samples were performed by comparing the degradation of MB in water under visible light ($\lambda > 420$ nm) irradiation. In a typical process, 10 mg of catalyst sample was added to 30 mL of 1.33×10^{-5} M aqueous solution of MB dye, and the mixture was stirred under dark for 1 h to reach the adsorption equilibrium because adsorption of dye on a catalyst's surface plays a crucial role for organic pollutant degradation.[48,49] After that, 2.5 mL of the mixture was taken out and centrifuged to separate the catalyst. The absorbance of the dye solution was measured to get the initial concentration of the dye before photocatalysis (C_0). Then, the solution was irradiated with a 300 W xenon lamp fitted with a 1.5 G filter and 420 nm cutoff filter. The absorption band of MB at 663 nm was monitored taking out aliquots from the reaction mixture after certain time intervals to get the concentration (C) of MB dye at that time. An ice cold water bath was used to stop evaporation of water during catalysis and to rule out degradation due to heating. The degradation efficiency was calculated using the following equation

$$\text{Degradation}\,(\%) = (1 - C/C_0) \times 100\% \qquad (1)$$

where C_0 is the concentration of MB at adsorption equilibrium and C is the residual concentration of MB at different time intervals.

The photodegradation of MB follows a pseudo-first-order kinetics, which can be expressed as

$$\ln(C_0/C) = kt \qquad (2)$$

where k (min $^{-1}$) is the degradation rate constant. Controlled experiments with only MB dye solution without catalyst and in the presence of catalyst without light irradiation were performed, and no significant degradation of the MB solution was observed in those reactions.

Hydroxyl radicals ($OH^{\bullet}$) produced during the photocatalysis under visible light irradiation was estimated by the fluorescence method using terephthalic acid (TA) as a probe molecule. In a typical process,[20] a 10 mg portion of the catalyst sample was dispersed in 30 mL of 5×10^{-4} M TA and diluted aqueous NaOH (2×10^{-3} M) solution. The resulting suspension was then exposed to visible light irradiation. At regular intervals, 2.5 mL of the suspension was collected and centrifuged to measure the maximum fluorescence emission intensity with an excitation wavelength of 315 nm. This method relies on the fluorescence signal at 425 nm of the 2-hydroxyterephthalic acid (TAOH).

RESULTS AND DISCUSSION

Structural Characterization. X-ray diffraction (XRD) study is performed for analyzing the crystal phase of as-synthesized pure and hybrid systems. Figure 1 shows the XRD plots of CdS NP, CdS NR, CdS NS, and their RGO composites. Figure 1 (plots a and b) shows the XRD patterns of pure CdS NP and CdS NP/RGO composites. The typical diffraction peaks are found at 2θ values of 26.80, 44.22, and 52.16° corresponding to (111), (220), and (311) planes of CdS NP, respectively, indicating that the CdS nanoparticles are of cubic zinc blend structure according to JCPDS file 10-454. For NR and the NR/RGO composite (plots c and d in Figure 1), the sharp peaks with high intensity at 2θ values of 25.11, 26.82, 28.47, 44.00, 48.29, and 52.16° are observed for (100), (002), (101), (110), (103), and (112) planes, confirming the hexagonal phase (JCPDS No. 41-1049) of CdS NR. In case of CdS NS (plot 1e), the growth of nanocrystal takes place along (002) plane which is confirmed by a sharp peak at a 2θ value of 26.84°, compared to other peaks at 2θ values of 44.00, 48.51, and 52.16° for (110), (103), and (112) crystal planes, respectively. This corresponds to the hexagonal phase of CdS,[16] and the same XRD pattern is found for the NS/RGO composites (plot f in Figure 1). Thus, the XRD study suggests that the phase and morphology of CdS nanostructures remain unchanged after hydrothermal treatment of the CdS−GO systems during preparation of CdS/RGO composites. XRD study confirms that the crystallinity of CdS nanocrystals is slightly better in composite systems. It is already reported[23,50] that the crystallinity of CdS nanocrystals is increased in the presence of graphene due to mechanical support.

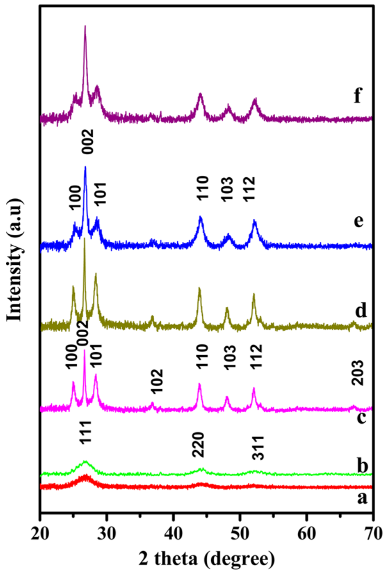

Figure 1. XRD plots of CdS NP (a), NR (c), NS (e), and their corresponding RGO composites (b, d, and f, respectively).

TEM measurement is performed to investigate the detailed structure of the synthesized nanostructures and their composites. Figure 2 shows the TEM images of the CdS NP, CdS NR, CdS NS, and their corresponding RGO composites. Synthesized CdS nanoparticles are uniform in size, and the

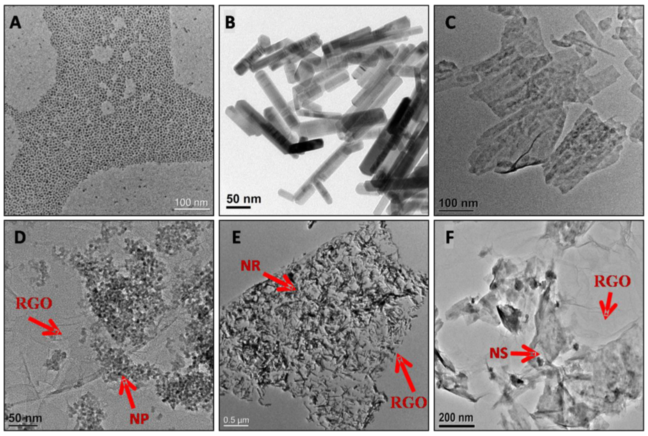

Figure 2. TEM images of CdS NP (A), NR (B), and NS (C) and their corresponding RGO composites (D−F).

diameter of the nanoparticles is ∼5−6 nm (Figure 2A). It can be seen from Figure 2B that the average length and diameter of 1D NR are 100 and 20 nm, respectively, with an aspect ratio of 5. Figure 2C shows the well-dispersed nanosheets having a lateral size of 100−300 nm. The thickness of the nanosheets was measured to be 5−7 nm from AFM analysis (Figure S1, Supporting Information). These nanostructures were surface-functionalized by 4-ATP, and the morphology remains unaltered after surface modification (Figure S2A−C, Supporting Information). These positively functionalized nanostructures were electrostatically attached with negatively charged GO to obtain composites with RGO, followed by hydrothermal reduction. It can be clearly seen from TEM images (Figure 2D−F and Figure S2D−F, Supporting Information) that NP, NR, and NS are well stacked on the RGO surface. The size and morphology of the nanostructures remain unaltered after the hydrothermal reduction of GO to RGO. It should be mentioned that CdS NPs are found to be aggregated in the composite systems after attachment with RGO. For further clarification, we have taken a dark-field STEM image and the corresponding elemental mapping of the NS/RGO hybrid (Figure S3, Supporting Information). It clearly indicates that a 2D nanosheet of CdS successfully grafted on another 2D sheet of RGO. It is seen from TEM images that CdS NP, NR, and NS are successfully attached on the RGO surface without any change of morphology.

We have modified the synthesized CdS NP, NR, and NS surfaces by 4-aminothiophenol (4-ATP) molecules for attachment with the GO surface. Surface modifications of the nanostructures are confirmed by FTIR study. Figure 3 shows the IR spectra of CdS NP (plot a), NR (plot b), NS (plot c), and pure 4-ATP (plot d). CdS has higher affinity toward the −SH group; thus, the −SH group of the 4-ATP molecule will bind with the CdS surface during ligand exchange. Weak S−H stretching frequency at 2548 cm^{-1} of the 4-ATP molecule disappears after binding with CdS. The characteristic bands at 1622 and 1490 cm^{-1} of the aromatic ring confirm the presence of the 4-ATP molecule on the surface of CdS nanostructures. The N−H stretching bands at 3363 and 3442 cm^{-1} become broadened, and the O−H band appears due to protonation of NH_2.[51] It is confirmed from the XPS data analysis that 4-ATP is attached with the CdS surface (Figure 3B and Figure S4, Supporting Information). The 2p peak of S for 4-ATP capped CdS NS can be fitted by two sets: a lower energy set of 161.4 and 163.02 eV is assigned to sulfur in the CdS crystal and a higher energy set of 162.1 and 163.78 eV is attributed to thiolate bound to the surface of CdS nanocrystals, which confirms the attachment of 4-ATP on the CdS surface.[52]

The protonation of the NH_2 group was confirmed by the zeta potential measurement of the 4-ATP-functionalized nanoparticles. The zeta potential values are found to be +38.4, +10.08, and +15.1 mV for CdS NP, NR, and NS samples, which are shown in Figure S5 in the Supporting Information. This positive potential of the CdS surface facilitates the electrostatic interaction with the negatively charged graphene oxide (−25 mV) surface, giving rise to CdS−GO composites.

UV−vis diffuse reflectance spectra (DRS) of CdS nanocrystals and their composites with RGO are shown in Figure 4A. The absorption band edges are 484, 525, and 515 nm, for pure CdS NP, CdS NR, and CdS NS, respectively. A significant enhancement of absorption spectra in the visible region is observed for all CdS nanostructures after attachment with RGO. This enhanced absorption in the visible region will be effective for light harvesting applications of the CdS−RGO composite system. Photoluminescence spectra are given in Figure 4B, and the band edge emissions at around 495 and 519 nm are observed for NP and NR after excitation at 375 nm. CdS NS shows a broad emission at 498 nm, which is assigned as band-gap emission. A significant photoluminescence quenching is also observed in all hybrid systems, indicating

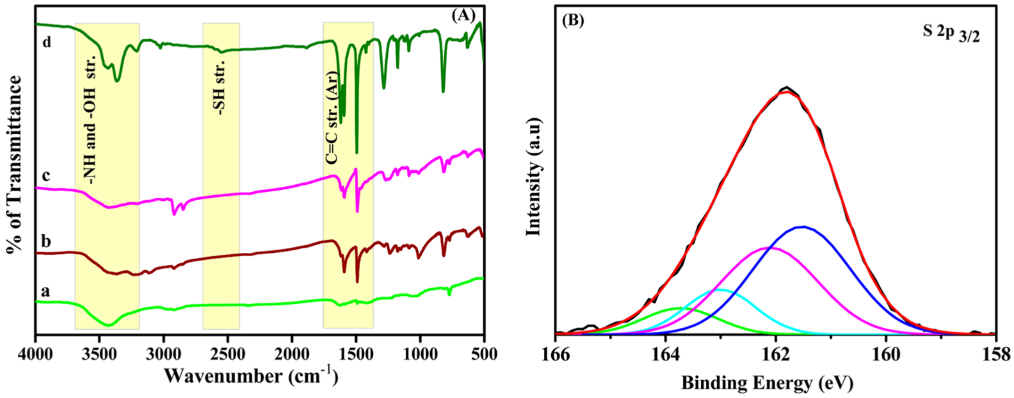

Figure 3. (A) IR spectra of ATP-functionalized CdS NP (a), NR (b), and NS (c) and pure ATP (d). (B) Deconvoluted XPS data of S 2p peak of CdS NS.

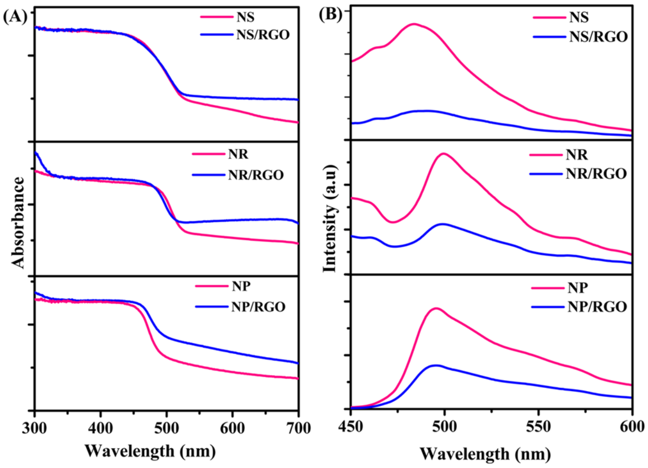

Figure 4. (A) Diffused reflectance spectra (DRS) of the pure CdS NP, NR, NS, and their composites. (B) Photoluminescence spectra of pure CdS NP, NR, NS, and their composites at excitation of 375 nm.

the possibility of excited-state electron transfer from CdS to RGO.

Raman studies of the pure and composite samples were performed to understand the electronic interaction between CdS nanostructures with RGO sheets. All the measurements were carried out at the excitation of 514 nm. The Raman spectrum of the CdS nanocrystals consists of characteristic CdS peaks, whereas the composite systems exhibit both the CdS and the RGO peaks. Figure 5A shows the Raman peaks of the CdS nanoparticle (plot a), nanorod (plot c), nanosheet (plot e), and their composites (plots b, d, and f), respectively. All the Raman spectra of CdS nanocrystals are composed of the characteristic fundamental longitudinal optical (1LO) mode at 300 cm^{-1} and first overtone (2LO) at around 600 cm^{-1}. A very weak second overtone at 900 cm^{-1} is observed for NR and NS samples. The peak position of 1LO and 2LO remains unchanged with variation of nanocrystal morphology from particle to rod to sheet, which is in consistent with the previous results.[53,54] The intensity ratio of 2LO to 1LO (2LO/1LO) provides an indication of the strength of electron-vibration coupling, which is found to increase while varying the morphology from NP to NR to NS. The 2LO/1LO ratio was found to be 0.22, 0.25, and 0.37 for CdS NP, NR, and NS, respectively. The smaller value of the ratio for NP is due to exciton confinement compared to NR and NS nanocrystals.[54] For the nanosheet structure, the exciton separation becomes larger due to the thin sheet structure of the nanocrystals leading to effective coupling between exciton and fundamental longitudinal phonon.[55] The ratio increases after attachment of nanocrystals with RGO, and the ratio was found to be 0.25, 0.44, and 0.58 for NP/RGO, NR/RGO, and NS/RGO composites. This increment of the 2LO/1LO ratio in the NS/RGO composite is attributed to extended interaction between 2D CdS NS with the 2D RGO sheets. The sheetlike nature of both CdS NS and RGO facilitates the effective area of interaction, leading to transfer of photogenerated electrons from CdS to RGO. Thus, the effective exciton separation in CdS NS occurs due to electron transfer to RGO. Raman study suggests that the strong interaction between CdS NS and RGO enhances photochemical properties.

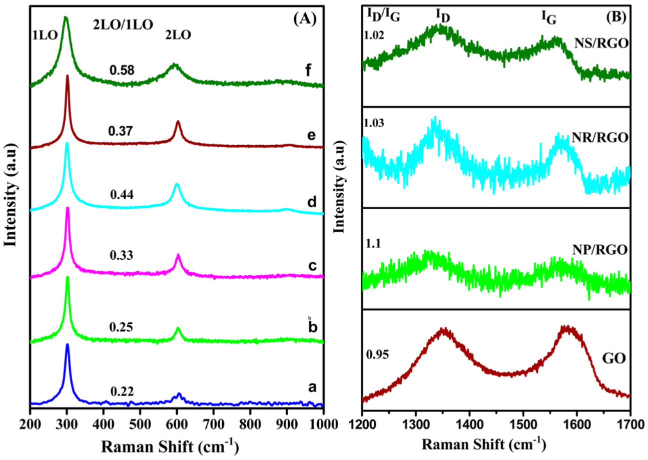

Figure 5. (A) Raman spectra of CdS NP, NR, NS (a, c, e), and their composites with RGO (b, d, f) showing CdS bands, (B) Raman spectra of pure GO and RGO composites of NP, NR, and NS showing graphene bands.

Figure 5B shows the Raman spectra of GO and CdS/RGO composite samples. GO shows two characteristic D and G[45,56,57] bands at 1350 and 1585 cm^{-1} with an intensity ratio (I_D/I_G) of 0.95. The G band is red-shifted to 1572, 1574, and 1567 cm^{-1}, and also the I_D/I_G ratio increases to 1.1, 1.03, and 1.02 for NP/RGO, NR/RGO, and NS/RGO composites, respectively, after composite formation with CdS nanocrystals. The red-shifting of the G band and the increase in the I_D/I_G ratio reveal that GO is reduced successfully and the native sheet structure of the graphene is restored in the composite systems.

Photocatalytic Study. The electron transfer from the CdS nanocrystal to RGO in the composite system was used for effective and enhanced degradation of Methylene Blue (MB) dye molecules under visible light ($\lambda > 420$ nm) irradiation. To monitor the photodegradation of MB molecules, the concentration of MB was plotted as a function of irradiation time. Figure 6 shows the plot of C/C_0 of MB vs time for pure CdS nanostructures and RGO composites. It is seen from plots that the relative photodegradation of a composite system is higher than that of the pure system. After 60 min of visible light irradiation, the photodegradation efficiencies of NP, NR, and NS are found to be 45.9, 62, and 79%, respectively, whereas the

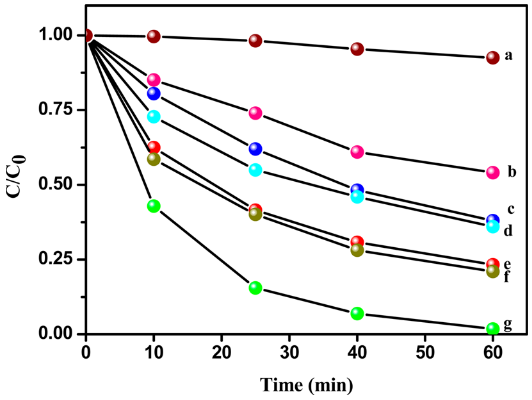

Figure 6. Photodegradation of MB dye under visible light where C_0 and C are the initial concentration and concentration of MB after irradiation of light in the corresponding time interval, in the absence of catalyst (a) and in the presence of NP (b), NR (c), NP/RGO (d), NR/RGO (e), NS (f), and NS/RGO (g) catalysts.

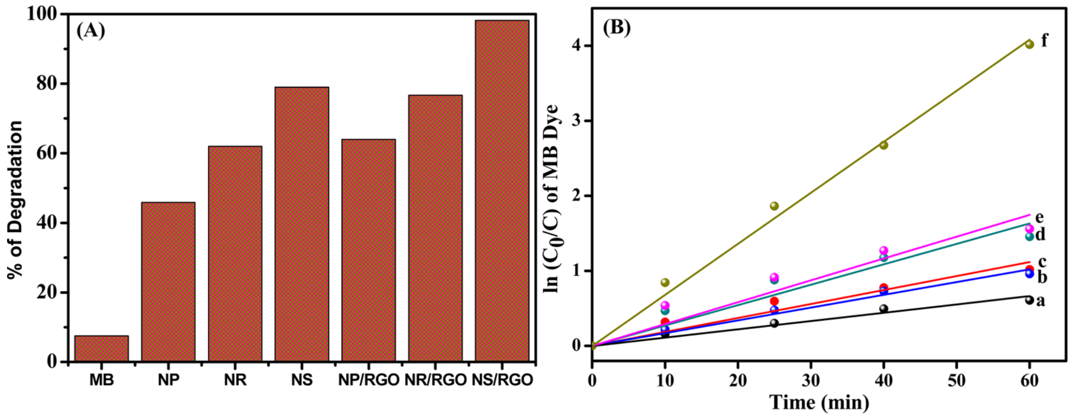

Figure 7. (A) Comparison of dye degradation efficiency after 60 min of light irradiation. (B) Plot of $\ln(C_0/C)$ as a function of irradiation time for photocatalysis of MB solution containing NP (a), NR (b), NR/RGO (d), NP/RGO (c), NS (e), and NS/RGO (f).

Table 1. Catalytic Efficiencies and Rate Constants of Different CdS Nanostructures and Their RGO Composites

	NP	NP/RGO	NR	NR/RGO	NS	NS/RGO
photocatalytic efficiency (%)	45.9	64.2	62	76.7	79	98.2
rate constant (min^{-1}) (error)	0.011 (0.0006)	0.018 (0.0013)	0.019 (0.0005)	0.02 (0.002)	0.027 (0.002)	0.068 (0.002)

efficiencies are found to be 64, 77, and 98% for NP/RGO, NR/RGO, and NS/RGO composites, respectively.

The degradation efficiencies of different catalysts are shown in Figure 7A. The maximum efficiency is found for the NS/RGO composite system. The kinetics of degradation of MB under visible light irradiation was studied by plotting $\ln(C_0/C)$ and reaction time. Figure 7B shows a linear relationship between $\ln(C_0/C)$ and reaction time, indicating a pseudo-first-order reaction kinetics of photodegradation of the MB molecule. The apparent rate constants are found to be 0.011, 0.019, 0.027, 0.018, 0.02, and 0.068 min^{-1} for CdS NP, CdS NR, CdS NS, NP/RGO, NR/RGO, and NS/RGO samples, respectively. We have carried out controlled experiment for comparison of catalytic activities between composite systems and a physical mixture of graphene and CdS NS, which are given in Figure S6 (Supporting Information). The rate of degradation is found to be 0.034 min^{-1} for the physical mixture of NS/RGO system, whereas the rate of degradation is 0.068 min^{-1} for the NS/RGO composite. Catalytic efficiency values and the rate constant of different systems are summarized in Table 1.

From the above results, it is clear that the photocatalytic activities of the CdS composites with RGO samples are higher compared to respective CdS nanostructures. The catalytic activity of the CdS NS/RGO composite is found to be ~4 times higher than that of NP/RGO and 3.4 times higher than that of NR/RGO composite samples. The CdS NS/RGO composite is found to be ~2.5 times more active than pure CdS NS samples. The recyclability of the NS/RGO system was examined, and the catalytic efficiency is found to be 77% after the third cycle of catalysis (Supporting Information, Figure S7).

Photocatalysis of this type of hybrid system depends on the extent of charge separation upon irradiation of light and intimate interfacial distance between semiconductor and graphene and also the crystal structure of different CdS nanocrystals. On the basis of this photocatalytic performance of the composite systems, the possible explanation for enhanced activity of the CdS NS/RGO system is given. During photocatalysis, upon irradiation of visible light, an electron is excited from the valence band to the conduction band of CdS NS. This photogenerated electron is transferred to the reduced graphene surface, and the adsorbed O_2 converts to $O_2^{\cdot -}$ active species, which generates a $OH^{\bullet}$ radical (confirmed by experiment which is discussed later) and consequently decomposes MB dye molecules. On the other hand, holes in the valence band oxidize dye molecules by capturing electrons from other dye molecules. A schematic representation of the mechanism is shown in Scheme 2. Maximum light-induced catalysis take places on the nanocrystal surface. It is expected that the nanorod (NR) exhibits better activity than the nanoparticle (NP) and nanosheet (NS) due to high crystallinity and the one-dimensional nature, which assists the migration of charge from one side to another side. The unexpected enhancement of the NS/RGO composite may be attributed to their unique 2D structural feature. The effective surface area

Scheme 2. Schematic Representation of MB Dye Degradation by CdS NS/RGO Composite

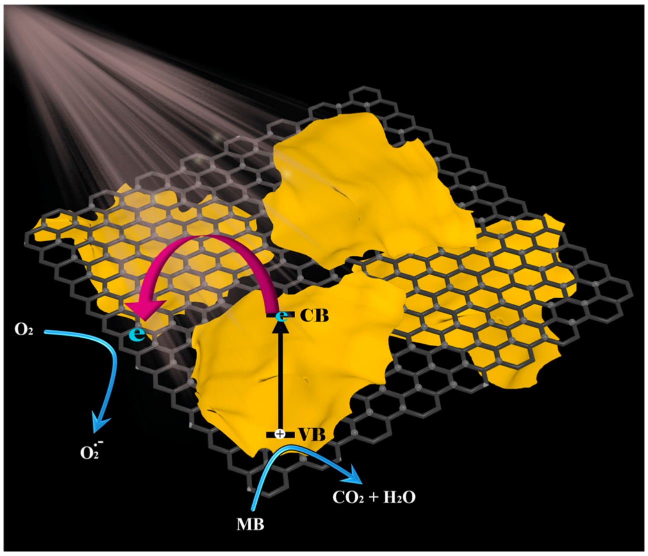

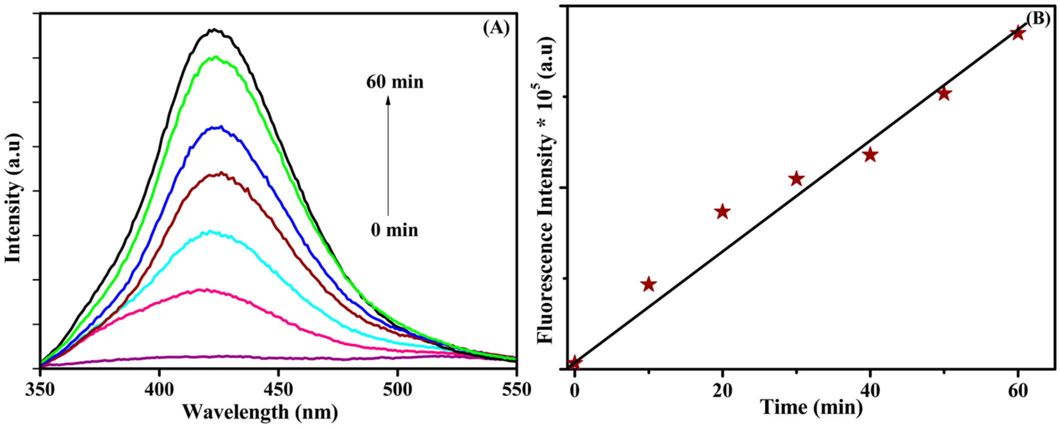

Figure 8. (A) Fluorescence intensity changes with time of the NS−RGO composite in a basic solution of terephthalic acid mixture under light irradiation. (B) Fluorescence intensity at 425 nm against illumination time for TAOH.

(Supporting Information, Figure S8) is 38, 64.5, and 86 $m^2 g^{-1}$ for NP, NR, and NS, respectively. It was found that the thin sheet structure has a large specific surface area for visible light harvesting and adsorbed more reactant molecules. Furthermore, the larger number of photogenerated charge carriers transfer from the exciton center to the reacting sites of RGO due to the very low thickness of NS, and the surface contact area between 2D NS and its 2D analogue RGO is very much larger than the other 0D or 1D nanostuctures. In our previous work, it is seen that the surface coverage by CdTe quantum dots (QDs) in the GO sheet influences the rate of electron transfer from QD to GO surface.[45] Thus, the effective separation of electron and hole occurs in the NS/RGO composite, which is consistent with Raman analysis. In addition, the lowering photocatalytic activity of CdS NP and its composite may be due to the cubic structure, which is consistent with previous reports[58,59] that the hexagonal structure exhibits better photocatalytic activity than the zinc blend cubic structure.

Photoinduced catalysis of these systems proceeds via $OH^{\bullet}$ radical formation in reaction medium. To recognize the presence of $OH^{\bullet}$ radicals, we have done a typical experiment using terephthalic acid (TA) as a probe, which reacts with reactive $OH^{\bullet}$ radicals and generates 2-hydroxyterephthalic acid (TAOH), a fluorescence active species.[20] The fluorescence intensity of TAOH is proportional to the amount of $OH^{\bullet}$ radicals produced under visible light illumination. Upon excitation at 315 nm, the maximum intensity at 425 nm was measured at 10 min time intervals. It is seen from Figure 8A that fluorescence intensity gradually increases with increasing irradiation time. This consequence indicates that the $OH^{\bullet}$ radical is definitely produced at the time of photocatalysis. Figure 8B shows that the fluorescence intensity at 425 nm linearly increases with irradiation time.

We have also performed parallel experiments in the absence of light and without catalyst, where no significant fluorescence enhancement was observed. This study reveals that only a catalyst generates $OH^{\bullet}$ radicals under visible light illumination, which degrades the pollutant molecules. We have performed LC−MS study to identify the oxidative degradation intermediate in solution in the presence of NS/RGO as catalyst under light illumination. The intensity of MB peaks decreases and generates some new peaks of degraded products after 30 min. The probable intermediate products were illustrated in the Supporting Information (Figures S9 and S10). Taking this into account, the probable mechanism of photocatalysis in this system is given below:

$$\mathrm{CdS} + h\nu \rightarrow \mathrm{CdS}\,(\mathrm{e}^{-}{}_{\mathrm{CB}}...h^{+}{}_{\mathrm{VB}})$$

$$\mathrm{CdS}\,(\mathrm{e}^{-}{}_{\mathrm{CB}}) + \mathrm{RGO} \rightarrow \mathrm{RGO}\,(\mathrm{e}) + \mathrm{CdS}$$

$$\mathrm{RGO}\,(\mathrm{e}) + \mathrm{O_2} \rightarrow \mathrm{O_2}^{\bullet -} + \mathrm{RGO}$$

$$\mathrm{O_2}^{\bullet -} + \mathrm{H_2O} \rightarrow \mathrm{HO_2}^{\bullet} + \mathrm{OH}^{-}$$

$$\mathrm{HO_2}^{\bullet} + \mathrm{H_2O} \rightarrow \mathrm{OH}\cdot + \mathrm{H_2O_2}$$

$$2\mathrm{H_2O_2} \rightarrow 2\mathrm{OH}\cdot$$

$$\mathrm{OH}\cdot + \mathrm{MB} \rightarrow \mathrm{CO_2} + \mathrm{H_2O}$$

$$\mathrm{CdS}\,(\mathrm{h}^{+}{}_{\mathrm{VB}}) + \mathrm{MB} \rightarrow \text{Degraded products}$$

■ CONCLUSION

In this report, we have synthesized grapheme oxide−CdS (nanoparticle, nanorod, and nanosheet) composites and investigated the influence of dimension of CdS nanocrystals on photocatalytic properties of these composites. Structural characterization has been done by XRD, TEM, FTIR, UV−vis, and Raman analysis. Electronic interaction is found to be strong in the case of RGO and CdS nanosheet. The photocatalytic activity of these composites has been estimated by degradation of Methylene Blue dye under constant visible light irradiation. It is observed that the CdS nanosheet/RGO composite exhibits significantly higher photocatalytic activity compared to nanorods and nanoparticle composites. Dimensionality-dependent photocatalytic activity could pave the way for developing new challenging catalytic materials.

■ ASSOCIATED CONTENT

Ⓢ Supporting Information

AFM image of CdS NS; TEM and HRTEM images of CdS nanoparticles, nanorods, and nanosheets and their composites with RGO; elemental analysis and mapping of NS/RGO hybrid system; XPS of CdS-4ATP; zeta potential of the surface-functionalized CdS nanocrystals; reusability of the catalyst; BET surface area plots of different CdS nanocrystals; comparison of photocatalysis between NS/RGO composite, NS/RGO physical mixture, and NS; LC−MS spectra; and probable intermediate products formed during photocatalytic degradation of MB are given in the Supporting Information. The Supporting Information is available free of charge on the ACS Publications website at DOI: 10.1021/acsami.5b03800.

AUTHOR INFORMATION

Corresponding Author

*E-mail: msap@iacs.res.in. Phone: (91)-33-2473-4971. Fax: (91)-33-2473-2805.

Notes

The authors declare no competing financial interest.

ACKNOWLEDGMENTS

SERB-DST is gratefully acknowledged for the financial support. R.B. thanks CSIR and S.K. thanks IACS for awarding the fellowship. We thank Mr. Gopal Krishna Manna for the graphic design.

REFERENCES

(1) Sadhu, S.; Tachiya, M.; Patra, A. A Stochastic Model for Energy Transfer from CdS Quantum Dots/Rods (Donors) to Nile Red Dye (Acceptors). *J. Phys. Chem. C* **2010**, *114*, 2842−2842.

(2) Yu, D.; Park, K.; Durstock, M.; Dai, L. Fullerene-Grafted Graphene for Efficient Bulk Heterojunction Polymer Photovoltaic Devices. *J. Phys. Chem. Lett.* **2011**, *2*, 1113−1118.

(3) Bang, J. H.; Kamat, P. V. CdSe Quantum Dot−Fullerene Hybrid Nanocomposite for Solar Energy Conversion: Electron Transfer and Photoelectrochemistry. *ACS Nano* **2011**, *5*, 9421−9427.

(4) Barman, M. K.; Bhattacharyya, S.; Patra, A. Steady State and Time Resolved Spectroscopic Study of C-dots-MEH-PPV Polymer Nanoparticles Composites. *Phys. Chem. Chem. Phys.* **2013**, *15*, 16834−16840.

(5) Golberg, D.; Bando, Y.; Huang, Y.; Terao, T.; Mitome, M.; Tang, C.; Zhi, C. Boron Nitride Nanotubes and Nanosheets. *ACS Nano* **2010**, *4*, 2979−2993.

(6) Zhang, Y.; Tang, Z.-R.; Fu, X.; Xu, Y.-J. Engineering the Unique 2D Mat of Graphene to Achieve Graphene-TiO_2 Nanocomposite for Photocatalytic Selective Transformation: What Advantage does Graphene Have over Its Forebear Carbon Nanotube? *ACS Nano* **2011**, *5*, 7426−7435.

(7) Dai, L. Functionalization of Graphene for Efficient Energy Conversion and Storage. *Acc. Chem. Res.* **2012**, *46*, 31−42.

(8) Geim, A. K.; Novoselov, K. S. The Rise of Graphene. *Nat. Mater.* **2007**, *6*, 183−191.

(9) Bonaccorso, F.; Sun, Z.; Hasan, T.; Ferrari, A. C. Graphene Photonics and Optoelectronics. *Nat. Photonics.* **2010**, *4*, 611−622.

(10) Peining, Z.; Nair, A. S.; Shengjie, P.; Shengyuan, Y.; Ramakrishna, S. Facile Fabrication of TiO_2−Graphene Composite with Enhanced Photovoltaic and Photocatalytic Properties by Electrospinning. *ACS Appl. Mater. Interfaces* **2012**, *4*, 581−585.

(11) Kamat, P. V. Graphene-Based Nanoassemblies for Energy Conversion. *J. Phys. Chem. Lett.* **2011**, *2*, 242−251.

(12) Khanchandani, S.; Kundu, S.; Patra, A.; Ganguli, A. K. Shell Thickness Dependent Photocatalytic Properties of ZnO/CdS Core−Shell Nanorods. *J. Phys. Chem. C* **2012**, *116*, 23653−23662.

(13) Tada, H.; Ishida, T.; Takao, A.; Ito, S. Drastic Enhancement of TiO_2-Photocatalyzed Reduction of Nitrobenzene by Loading Ag Clusters. *Langmuir* **2004**, *20*, 7898−7900.

(14) Rao, C. N. R.; Govindaraj, A. Synthesis of Inorganic Nanotubes. *Adv. Mater.* **2009**, *21*, 4208−4233.

(15) Gautam, U. K.; Fang, X.; Bando, Y.; Zhan, J.; Golberg, D. Synthesis, Structure, and Multiply Enhanced Field-Emission Properties of Branched ZnS Nanotube−In Nanowire Core−Shell Heterostructures. *ACS Nano* **2008**, *2*, 1015−1021.

(16) Xu, Y.; Zhao, W.; Xu, R.; Shi, Y.; Zhang, B. Synthesis of Ultrathin CdS Nanosheets as Efficient Visible-Light-Driven Water Splitting Photocatalysts for Hydrogen Evolution. *Chem. Commun.* **2013**, *49*, 9803−9805.

(17) Sagawa, T.; Yoshikawa, S.; Imahori, H. One-Dimensional Nanostructured Semiconducting Materials for Organic Photovoltaics. *J. Phys. Chem. Lett.* **2010**, *1*, 1020−1025.

(18) Yu, Y.; Zhang, P.; Guo, L.; Chen, Z.; Wu, Q.; Ding, Y.; Zheng, W.; Cao, Y. The Design of TiO_2 Nanostructures (Nanoparticle, Nanotube, and Nanosheet) and Their Photocatalytic Activity. *J. Phys. Chem. C* **2014**, *118*, 12727−12733.

(19) Kim, I. Y.; Jo, Y. K.; Lee, J. M.; Wang, L.; Hwang, S.-J. Unique Advantages of Exfoliated 2D Nanosheets for Tailoring the Functionalities of Nanocomposites. *J. Phys. Chem. Lett.* **2014**, *5*, 4149−4161.

(20) Khanchandani, S.; Kundu, S.; Patra, A.; Ganguli, A. K. Band Gap Tuning of ZnO/In_2S_3 Core/Shell Nanorod Arrays for Enhanced Visible-Light-Driven Photocatalysis. *J. Phys. Chem. C* **2013**, *117*, 5558−5567.

(21) Linsebigler, A. L.; Lu, G.; Yates, J. T. Photocatalysis on TiO_2 Surfaces: Principles, Mechanisms, and Selected Results. *Chem. Rev.* **1995**, *95*, 735−758.

(22) Schneider, J.; Matsuoka, M.; Takeuchi, M.; Zhang, J.; Horiuchi, Y.; Anpo, M.; Bahnemann, D. W. Understanding TiO_2 Photocatalysis: Mechanisms and Materials. *Chem. Rev.* **2014**, *114*, 9919−9986.

(23) Zhang, N.; Zhang, Y.; Pan, X.; Fu, X.; Liu, S.; Xu, Y.-J. Assembly of CdS Nanoparticles on the Two-Dimensional Graphene Scaffold as Visible-Light-Driven Photocatalyst for Selective Organic Transformation under Ambient Conditions. *J. Phys. Chem. C* **2011**, *115*, 23501−23511.

(24) Ma, R.-M.; Dai, L.; Qin, G.-G. High-Performance Nano-Schottky Diodes and Nano-MESFETs Made on Single CdS Nanobelts. *Nano Lett.* **2007**, *7*, 868−873.

(25) Fang, J.; Xu, L.; Zhang, Z.; Yuan, Y.; Cao, S.; Wang, Z.; Yin, L.; Liao, Y.; Xue, C. Au@TiO_2−CdS Ternary Nanostructures for Efficient Visible-Light-Driven Hydrogen Generation. *ACS Appl. Mater. Interfaces* **2013**, *5*, 8088−8092.

(26) Zhang, L. J.; Zheng, R.; Li, S.; Liu, B. K.; Wang, D. J.; Wang, L. L.; Xie, T. F. Enhanced Photocatalytic H_2 Generation on Cadmium Sulfide Nanorods with Cobalt Hydroxide as Cocatalyst and Insights into Their Photogenerated Charge Transfer Properties. *ACS Appl. Mater. Interfaces* **2014**, *6*, 13406−13412.

(27) Han, S.; Hu, L.; Gao, N.; Al-Ghamdi, A. A.; Fang, X. Efficient Self-Assembly Synthesis of Uniform CdS Spherical Nanoparticles-Au Nanoparticles Hybrids with Enhanced Photoactivity. *Adv. Funct. Mater.* **2014**, *24*, 3725−3733.

(28) Liu, S.; Zhang, N.; Tang, Z.-R.; Xu, Y.-J. Synthesis of One-Dimensional CdS@TiO_2 Core−Shell Nanocomposites Photocatalyst for Selective Redox: The Dual Role of TiO_2 Shell. *ACS Appl. Mater. Interfaces* **2012**, *4*, 6378−6385.

(29) Cao, A.; Liu, Z.; Chu, S.; Wu, M.; Ye, Z.; Cai, Z.; Chang, Y.; Wang, S.; Gong, Q.; Liu, Y. A Facile One-Step Method to Produce Graphene−CdS Quantum Dot Nanocomposites as Promising Optoelectronic Materials. *Adv. Mater.* **2010**, *22*, 103−106.

(30) Yuan, K.; Chen, L.; Tan, L.; Chen, Y. Performance Enhancement of Bulk Heterojunction Solar Cells with Direct Growth of CdS-Cluster-Decorated Graphene Nanosheets. *Chem.—Eur. J.* **2014**, *20*, 6010−6018.

(31) Zhang, N.; Yang, M.-Q.; Tang, Z.-R.; Xu, Y.-J. Toward Improving the Graphene−Semiconductor Composite Photoactivity via the Addition of Metal Ions as Generic Interfacial Mediator. *ACS Nano* **2014**, *8*, 623−633.

(32) Chen, Z.; Liu, S.; Yang, M.-Q.; Xu, Y.-J. Synthesis of Uniform CdS Nanospheres/Graphene Hybrid Nanocomposites and Their Application as Visible Light Photocatalyst for Selective Reduction of Nitro Organics in Water. *ACS Appl. Mater. Interfaces* **2013**, *5*, 4309−4319.

(33) Low, J.; Cao, S.; Yu, J.; Wageh, S. Two-Dimensional Layered Composite Photocatalysts. *Chem. Commun.* **2014**, *50*, 10768−10777.

(34) Liu, H.; Lv, T.; Wu, X.; Zhu, C.; Zhu, Z. Preparation and Enhanced Photocatalytic Activity of CdS@RGO Core−Shell Structural Microspheres. *Appl. Surf. Sci.* **2014**, *305*, 242−246.

(35) Johra, F. T.; Jung, W.-G. Effect of pH on the Synthesis and Characteristics of RGO−CdS Nanocomposites. *Appl. Surf. Sci.* **2014**, *317*, 1015−1021.

(36) Xiang, Q.; Yu, J.; Jaroniec, M. Graphene-Based Semiconductor Photocatalysts. *Chem. Soc. Rev.* **2012**, *41*, 782−796.

(37) Xie, G.; Zhang, K.; Guo, B.; Liu, Q.; Fang, L.; Gong, J. R. Graphene-Based Materials for Hydrogen Generation from Light-Driven Water Splitting. *Adv. Mater.* **2013**, *25*, 3820−3839.

(38) Zhang, J.; Yu, J.; Jaroniec, M.; Gong, J. R. Noble Metal-Free Reduced Graphene Oxide-$Zn_xCd_{1-x}S$ Nanocomposite with Enhanced Solar Photocatalytic H_2-Production Performance. *Nano Lett.* **2012**, *12*, 4584−4589.

(39) Xie, G.; Zhang, K.; Fang, H.; Guo, B.; Wang, R.; Yan, H.; Fang, L.; Gong, J. R. A Photoelectrochemical Investigation on the Synergetic Effect between CdS and Reduced Graphene Oxide for Solar-Energy Conversion. *Chem.—Asian. J.* **2013**, *8*, 2395−2400.

(40) Lee, J. S.; You, K. H.; Park, C. B. Highly Photoactive, Low Bandgap TiO_2 Nanoparticles Wrapped by Graphene. *Adv. Mater.* **2012**, *24*, 1084−1088.

(41) Pan, X.; Zhao, Y.; Liu, S.; Korzeniewski, C. L.; Wang, S.; Fan, Z. Comparing Graphene-TiO_2 Nanowire and Graphene-TiO_2 Nanoparticle Composite Photocatalysts. *ACS Appl. Mater. Interfaces* **2012**, *4*, 3944−3950.

(42) Xiao, F.-X.; Miao, J.; Liu, B. Layer-by-Layer Self-Assembly of CdS Quantum Dots/Graphene Nanosheets Hybrid Films for Photoelectrochemical and Photocatalytic Applications. *J. Am. Chem. Soc.* **2014**, *136*, 1559−1569.

(43) Li, Q.; Guo, B.; Yu, J.; Ran, J.; Zhang, B.; Yan, H.; Gong, J. R. Highly Efficient Visible-Light-Driven Photocatalytic Hydrogen Production of CdS-Cluster-Decorated Graphene Nanosheets. *J. Am. Chem. Soc.* **2011**, *133*, 10878−10884.

(44) Liu, S.; Chen, Z.; Zhang, N.; Tang, Z.-R.; Xu, Y.-J. An Efficient Self-Assembly of CdS Nanowires−Reduced Graphene Oxide Nanocomposites for Selective Reduction of Nitro Organics under Visible Light Irradiation. *J. Phys. Chem. C* **2013**, *117*, 8251−8261.

(45) Kundu, S.; Sadhu, S.; Bera, R.; Paramanik, B.; Patra, A. Fluorescence Dynamics and Stochastic Model for Electronic Interaction of Graphene Oxide with CdTe QD in Graphene Oxide-CdTe QD Composite. *J. Phys. Chem. C* **2013**, *117*, 23987−23995.

(46) Hummers, W. S.; Offeman, R. E. Preparation of Graphitic Oxide. *J. Am. Chem. Soc.* **1958**, *80*, 1339−1339.

(47) Sadhu, S.; Tachiya, M.; Patra, A. A Stochastic Model for Energy Transfer from CdS Quantum Dots/Rods (Donors) to Nile Red Dye (Acceptors). *J. Phys. Chem. C* **2009**, *113*, 19488−19492.

(48) Xu, Y.; Langford, C. H. UV- or Visible-Light-Induced Degradation of X_3B on TiO_2 Nanoparticles: The Influence of Adsorption. *Langmuir* **2001**, *17*, 897−902.

(49) Li, X.; Lv, K.; Deng, K.; Tang, J.; Su, R.; Sun, J.; Chen, L. Synthesis and Characterization of ZnO and TiO_2 Hollow Spheres with Enhanced Photoreactivity. *Mater. Sci. Eng., B* **2009**, *158*, 40−47.

(50) Yu, J.; Jin, J.; Cheng, B.; Jaroniec, M. A Noble Metal-Free Reduced Graphene Oxide-CdS Nanorod Composite for the Enhanced Visible-Light Photocatalytic Reduction of CO_2 to Solar Fuel. *J. Mater. Chem. A* **2014**, *2*, 3407−3416.

(51) Llusar, M.; Monros, G.; Roux, C.; Pozzo, J. L.; Sanchez, C. One-Pot Synthesis of Phenyl- and Amine-Functionalized Silica Fibers through the Use of Anthracenic and Phenazinic Organogelators. *J. Mater. Chem.* **2003**, *13*, 2505−2514.

(52) Turo, M. J.; Macdonald, J. E. Crystal-Bound vs Surface-Bound Thiols on Nanocrystals. *ACS Nano* **2014**, *8*, 10205−10213.

(53) Shiang, J. J.; Risbud, S. H.; Alivisatos, A. P. Resonance Raman Studies of the Ground and Lowest Electronic Excited State in CdS Nanocrystals. *J. Chem. Phys.* **1993**, *98*, 8432−8442.

(54) Zeiri, L.; Patla, I.; Acharya, S.; Golan, Y.; Efrima, S. Raman Spectroscopy of Ultranarrow CdS Nanostructures. *J. Phys. Chem. C* **2007**, *111*, 11843−11848.

(55) Hu, C.; Zeng, X.; Cui, J.; Chen, H.; Lu, J. Size Effects of Raman and Photoluminescence Spectra of CdS Nanobelts. *J. Phys. Chem. C* **2013**, *117*, 20998−21005.

(56) Stankovich, S.; Dikin, D. A.; Piner, R. D.; Kohlhaas, K. A.; Kleinhammes, A.; Jia, Y.; Wu, Y.; Nguyen, S. T.; Ruoff, R. S. Synthesis of Graphene-Based Nanosheets via Chemical Reduction of Exfoliated Graphite Oxide. *Carbon* **2007**, *45*, 1558−1565.

(57) Kudin, K. N.; Ozbas, B.; Schniepp, H. C.; Prud'homme, R. K.; Aksay, I. A.; Car, R. Raman Spectra of Graphite Oxide and Functionalized Graphene Sheets. *Nano Lett.* **2007**, *8*, 36−41.

(58) Chen, Y.; Huang, R.; Chen, D.; Wang, Y.; Liu, W.; Li, X.; Li, Z. Exploring the Different Photocatalytic Performance for Dye Degradations over Hexagonal $ZnIn_2S_4$ Microspheres and Cubic $ZnIn_2S_4$ Nanoparticles. *ACS Appl. Mater. Interfaces* **2012**, *4*, 2273−2279.

(59) Matsumura, M.; Furukawa, S.; Saho, Y.; Tsubomura, H. Cadmium Sulfide Photocatalyzed Hydrogen Production from Aqueous Solutions of Sulfite: Effect of Crystal Structure and Preparation Method of the Catalyst. *J. Phys. Chem.* **1985**, *89*, 1327−1329.